Processing, Characterization and Modeling of Non-Random Porous Ceramic Structures

Ashwin Hattiangadi and Amit Bandyopadhyay
School of Mechanical and Materials Engineering,
Washington State University,
Pullman, WA 99164

Abstract

Processing of non-random porous ceramic structures via fused deposition process is discussed. These structures are characterized experimentally and statistically based on their compressive strength. Finite element modeling is used to understand the effect of stress concentration leading to the strength degradation of these brittle elastic solids.

Introduction

Porous ceramic materials are of significant technological interest due to their applications in molten metal filters, light weight core for sandwich panels, radiant burners, catalyst supports, sensors and bone grafts [1-2]. The porosity may be needed in the structures to reduce the weight of the structure at the non-critical areas, to increase the activity of the ceramics by increasing surface area or to separate the wanted from the unwanted materials during filtering. But in all the cases, a better control of the pore geometry and improvements of the mechanical properties of the porous structures are important to improve the reliability of the structures.

Various processing techniques have been utilized to fabricate porous ceramic materials. Replamineform process was utilized to fabricate porous bioceramic implants to duplicate the macroporous microstructures of corals that have interconnected pores [3]. Porous alumina ceramics have been fabricated using pore former or foaming agent that evolves gases during sintering at elevated temperatures [4]. Porous Hydroxyapatite (HAp) ceramic blocks were also fabricated using HAp slurry mixed with foaming agent followed by sintering at elevated temperature [5]. Shrout et al. and Rittenmyer et al. [6-7] reported fabrication of 3-3 piezocomposites using a mixture of volatilizable plastic spheres and PZT powder, in a process known as BURPS (BURned-out Plastic Spheres). Unfortunately, all of these processes form structures with randomly arranged pores with a wide variety of sizes and have limited flexibility to control pore volumes and porosity distribution in the final structure. In this paper, we discuss about porous ceramics with non-random pore volumes, shapes and sizes, which have been processed using solid freeform fabrication (SFF) methods. SFF offers tremendous flexibility in varying the porosity parameters which controls the strength of these ceramic structures as well.

Theoretical and experimental characterization of porous materials is not new and several theories have already been postulated to characterize the mechanical strength of polycrystalline porous ceramics. These theories to characterize the mechanical strength can be classified into three broad categories: (1) reduction in cross-section area approach, (2) stress concentration approach and (3) effective flaw size approach. Most of these studies in predicting the porosity-strength relationship have been limited to the fitting capability of the equations towards the available experimental data and no attempt has been made to quantitatively access the effects of porosity parameters on the strength degradation of the porous ceramic structures.

The effects of porosity parameters such as size, shape, and pore interaction on the strength degradation of porous ceramics under uniaxial compression loading are presented. Finite element method (FEM) is used to study the effects based on stress concentration. Statistical analysis of the experimental results shows the main factors and the interaction among them that affect compressive strength.

Processing

Solid freeform fabrication (SFF) is an approach to directly build three-dimensional components layer-by-layer from a computer data description or a CAD file of a component. SFF techniques can be used in two ways to fabricate functional metal/ceramic prototypes: (a) direct and (b) indirect. In the direct route, green metal/ceramic components are directly fabricated using SFF. Recently, researchers modified the Fused Deposition process [8] to manufacture direct ceramic parts via a process known as FDC (Fused Deposition of Ceramics) [9, 10]. In the indirect route, the negative or the mold of the desired structure is fabricated via SFF. The positive is then cast using metal/ceramic powder based slurry via a lost mold technique. Recently, using the indirect processing route, 3D honeycomb porous ceramic preforms have been fabricated [11]. Commercially available Fused Deposition Modeling (model FDM 1650, Stratasys Inc., MN) process was used for making the molds. The indirect processing route is schematically shown in **Fig. 1** and the schematics of the wax mold is shown in **Fig. 2a** and **b**.

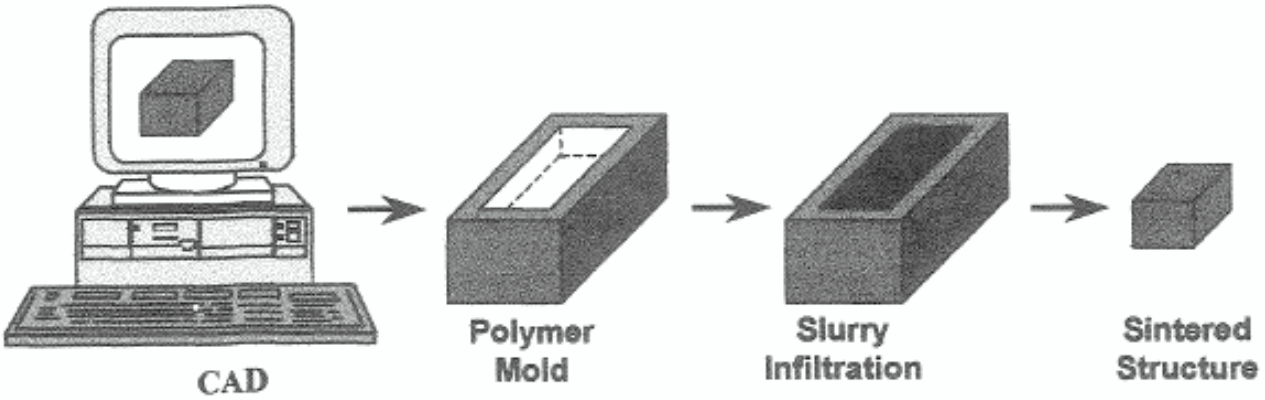

Fig.1: Schematic of the indirect processing of ceramic structures via rapid prototyping processes.

Thermoplastic polymeric molds were built using FDM 1650 machine. The raster gap (X and Y gap), road width (length a) and slice thickness (Z gap) were varied with respect to each other, to obtain desired pore size, pore shape and volume fraction porosity.

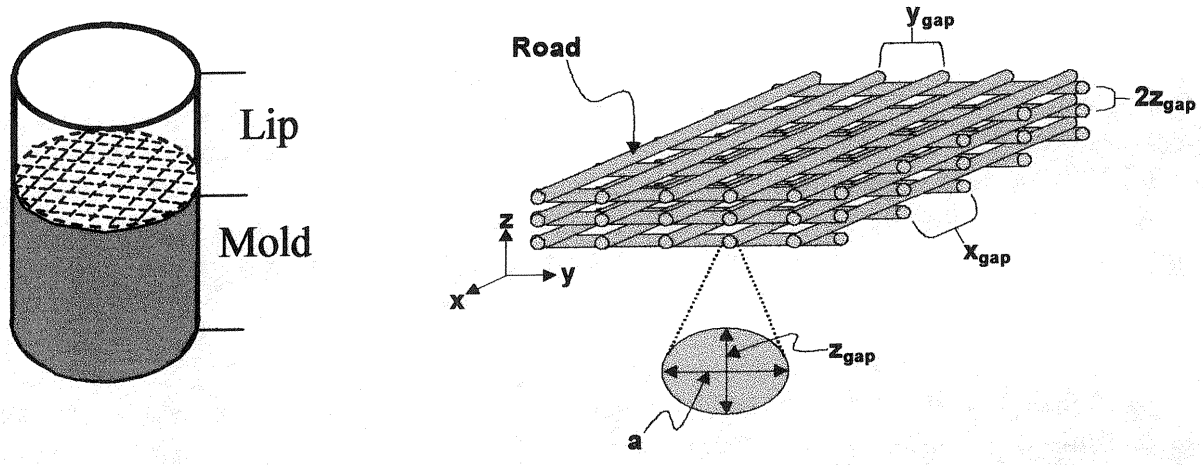

(a) (b)

Fig.2: **(a)** Schematic of polymeric mold design using FDM. **(b)** Schematic of internal wax pattern in the mold via FDM.

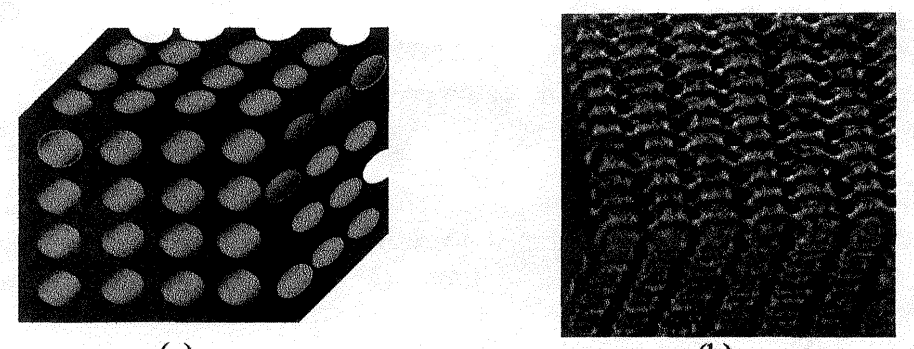

(a) (b)

Fig.3: Microstructures of 3D honeycomb porous ceramic structures. **(a)** Schematic; **(b)** Side view of a structure with uniform porosity

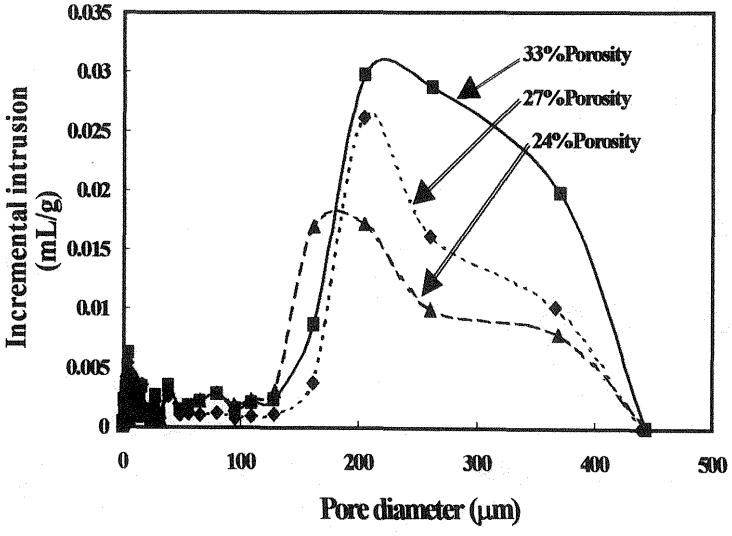

Fig.4(a): Hg-porosimetry plots show the porosity distribution in 3D honeycomb porous mullite ceramics

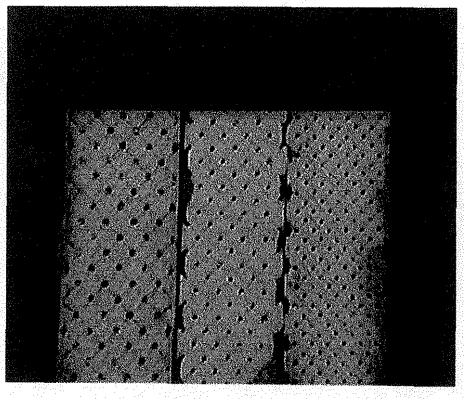

Fig. 4(b): 3D honeycomb porous ceramic structures with different volume fractions of porosity.

Fig. 3a shows the schematic of the porous structures and **Fig. 3b** is photomicrograph of the side view of porous 3D honeycomb ceramic preforms. In both the cases, it can be observed that pores are uniformly distributed and interconnected in all three directions. **Fig. 4a** shows the mercury porosimeter (model Autopore III, Micromeritrics, GA) plot of incremental intrusion of mercury in the porous structures. It can be seen from this plot that the maximum volume of the mercury, that intrudes the porous ceramic, occupies the macropores in the vicinity of 150 to 300 μm, which was actually the designed pore sizes for these structures. **Fig. 4b** shows the porous ceramic structures where the pore sizes and their distribution are varied.

Experimental Testing:

Experimental result for strength degradation of mullite ceramics subjected to compressive loads is discussed in this section. Some of the trends were observed that follow the exponential equation proposed first by Ryshekewitch [12]. The equation was expressed as

$$\sigma = \sigma_0 (\exp.)^{-bP}$$

where, σ, is the stress of the porous structure in compression.

σ_0, is the stress of non-porous structure.

b, empirical constant. Ryshekewitch (1953) determined the value of "b" from the slope of the curve as 6 to 9, for different loading conditions.

and P, is the volume fraction porosity for zirconia and alumina.

Cylindrical samples of 1-inch length and 0.6-inch diameter were fabricated having a non-random porous structure with predetermined pore size and pore volume. Uniaxial compressive tests were done on a servo-hydraulic load frame (MTS 4 post (44KN)) under displacement control at a stroke rate of 1.27 mm/min

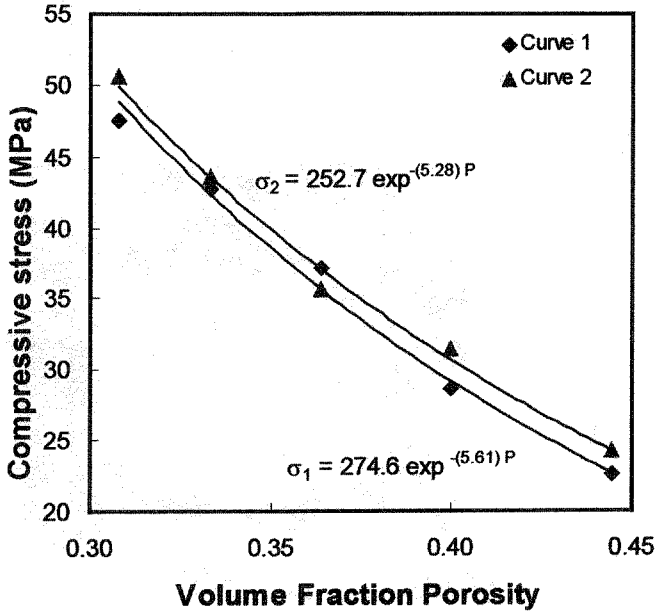

. **Fig. 5**: Variation of Raster Gap

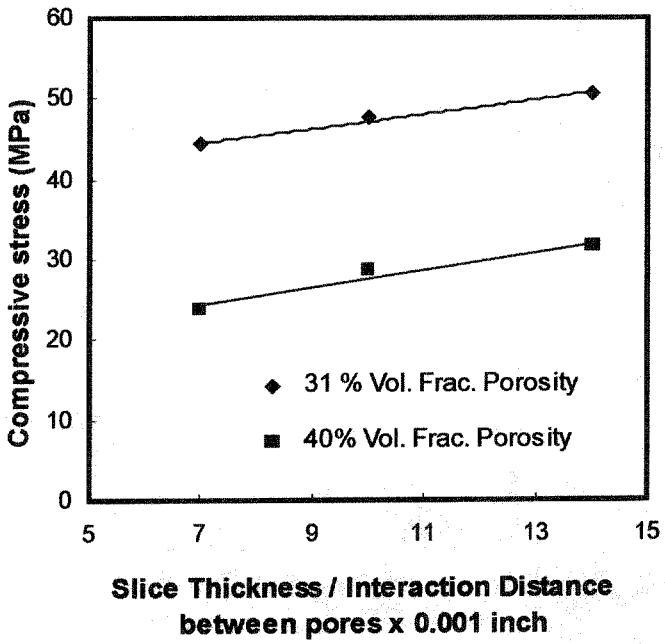

Fig. 6: Variation of Slice Thickness

By varying the raster gap (X and Y-gap in **Fig. 2b**) between the filaments in the wax mold, the interaction between pores in the horizontal plane of the ceramic structure was varied. This variation for different volume fraction porosities shows a failure trend in **Fig. 5** for which the exponential equation is a good fit. The Curve 1 and 2 in **Fig. 5** show the failure trend for two different pore heights which is achieved by varying the slice thickness (Z- gap in **Fig.2b**). The strength is slightly lesser when a smaller slice thickness is used, shown as curve 1 compared to curve 2, where a higher values of slice thickness was used. The σ_0 based on the above Ryshekewitch equation for curve 1 and 2 are 274.6 MPa and 252.7 MPa, respectively. The variation of the slice thickness or pore shape in the vertical direction is shown in detail in **Fig. 6** for 31% and 40% volume fraction porosities.

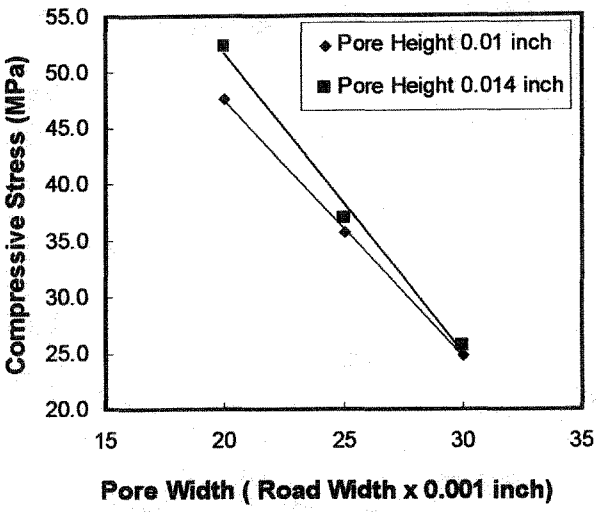

Fig. 7 : Variation of Road Width

It can be observed from **Fig. 6** that as the vertical interaction between the pores increase the strength decreases. It also suggests that as the pore shape becomes more elliptical in the vertical direction, the compressive strength decreases.

By varying the road width (length a in **Fig. 2b**) in the wax mold, the pore shape can also be changed along the horizontal direction as shown in **Fig. 7** for two slice thickness of .01 and .014 inch. The strength of the ceramic decreases as the pore width increases. In other words as the shape of the pore becomes more elliptical the strength decreases.

Statistical analysis

Analysis of Variance for the Compressive Strength Data					
Source of variation (	**A :- Sum of Squares of the Compressive data (Sq. MPa)**	**B :- Degrees of Freedom**	**C :- Mean Square = A / B**	**F-Value = C / Error**	**P-Value**
Road Width (RW)	894.26	1	894.26	27.585	Very Low
Raster Gap (RG)	370.52	1	370.52	11.429	Very Low
Road Width-Slice Th. (RW-ST)	30.60	1	30.60	0.944	High
Slice Thickness (ST)	16.17	1	16.17	0.499	High
Raster Gap - Slice Th. (RG -ST)	6.51	1	6.51	0.201	High
RG-RW-ST	0.26	1	0.26	0.008	Very high
Raster Gap - Road Width (RG-RW)	0.03	1	0.03	0.001	Very High
Sum of Squares (Error)	259.4	8	32.4		
Sum of Squares (Total)	1577.7	15			
Std. Error Regression Coeff.	1.16				
Standard Error Limits on the Effect Estimates	(plus / minus) 4.65				

Table 1: Two level-three factorial experimental analysis of variance

A two-level three factorial design of experiment was carried out on the basis of analysis of variance (ANOVA). The **Table 1** shows statistical analysis for the three main factors, raster gap(RG), road width (RW) and slice thickness(ST). The road width (RW) and raster gap (RG) are the most important controlling parameters of the strength of porous structures. Their F-values are very high indicating that these factors have most significant effect. The probability that these factors will not control the strength (P-value) is also very low.

Finite Element Modeling

Finite element modeling (FEM) of porous ceramics for increasing porosity and varying pore shapes was studied with respect to their effects on strength degradation of the structures under compressive loading. The FEM was carried out on ANSYS (ver.5.4). Representative cross-sectional schematics of typical porous ceramic structures with uniform pore shapes and sizes are shown in two dimensions in **Fig. 8a.**

Boundary conditions, plane stress method and material properties: In **Fig. 8a**, the nodes along the bottom edge are fixed in the Y-direction but are allowed to move in the X-direction. A node at one of the bottom corners is fixed in the X-direction to prevent rigid body motion. A load is applied to the mesh in the Y-direction "σ_y" such that it is compressive in nature. In controlled porosity ceramic structures, where long cylindrical pores in the third dimension are oriented parallel to the stress direction, there should not be any stress concentration effect, which has been observed by Boccaccini et al.[13] Hence, in this study, plane stress method is used where the stresses in the Z-direction are set to zero. The Young's modulus and Poisson's ratio are selected arbitrarily as 137.8 GPa (2 x 10^7 psi) and 0.1, respectively. The porous structure is represented by **Fig. 8a and b** in two-dimensions and the porosity is evaluated as area fraction.

Results and discussion of the FEM: All the finite element analysis (FEA) results are shown as a variation of stress concentration factors (SCF) with respect to different porosity parameters. SCF is calculated as σ_θ / σ along the perimeter of the pore, where the angle θ defines the location, σ is the applied stress and σ_θ is the stress at that specific location. The angle θ is zero for all the cases at the perimeter which intersects the y-axis ($\theta = 0$) and increases along the clockwise direction as shown in **Fig. 8a**.

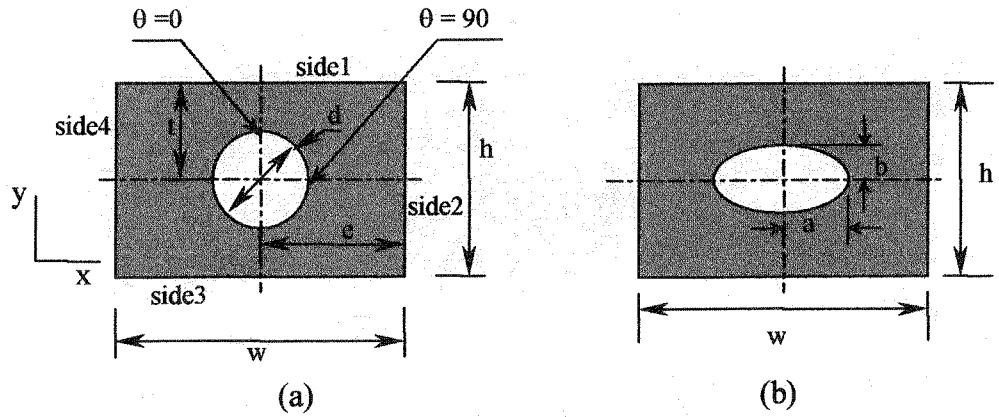

Fig. 8: **(a)** Finite plate with one pore **(b)** Plate with elliptical pore.

Effect of increasing porosity: The variation of tensile and compressive component of the SCF with volume fraction porosity is shown in **Fig. 9a.** This is a very ideal case and it may be difficult to manufacture porous structures with perfectly circular pores. The exponential increase of the tensile component does indicate that the strength is affected by the increasing porosity.

The experimental plot of **Fig. 5** obtained by varying the raster gap shows similar effect as the increase in porosity modeled using finite elements. In the experimental study we observed an exponential decrease in strength as the volume fraction porosity or the raster gap increased. In the FEM study, we observe an exponential increase in SCF as the volume fraction porosity increases.

Effect of pore shapes: The above structure was considered for circular/spherical pores. But in reality, all pores are seldom spherical. **Fig. 8c** shows a schematic diagram where the pore has an elliptical shape. The ellipticity of pores will vary as the ratio of the major and the minor axis (a and b respectively) changes. **Fig. 9b** shows the effect of pore shapes on SCF. With the increase in ellipticity of the pores, more severe stress concentration effects are observed. The cross sectional solid area decreases in one direction compared to the other and it has been shown that minimum solid area is one of the critical parameters that predicts the strength of the porous structures [14].

The effect of change in pore shape through this FEM study matches well with the experimental results shown by **Figs. 6 and 7**. Varying the slice thickness and road width has experimentally shown that by decreasing the pore ellipticity controlled porous structures with higher compressive strengths can be designed and this may be caused due to a decrease in stress concentration effects.

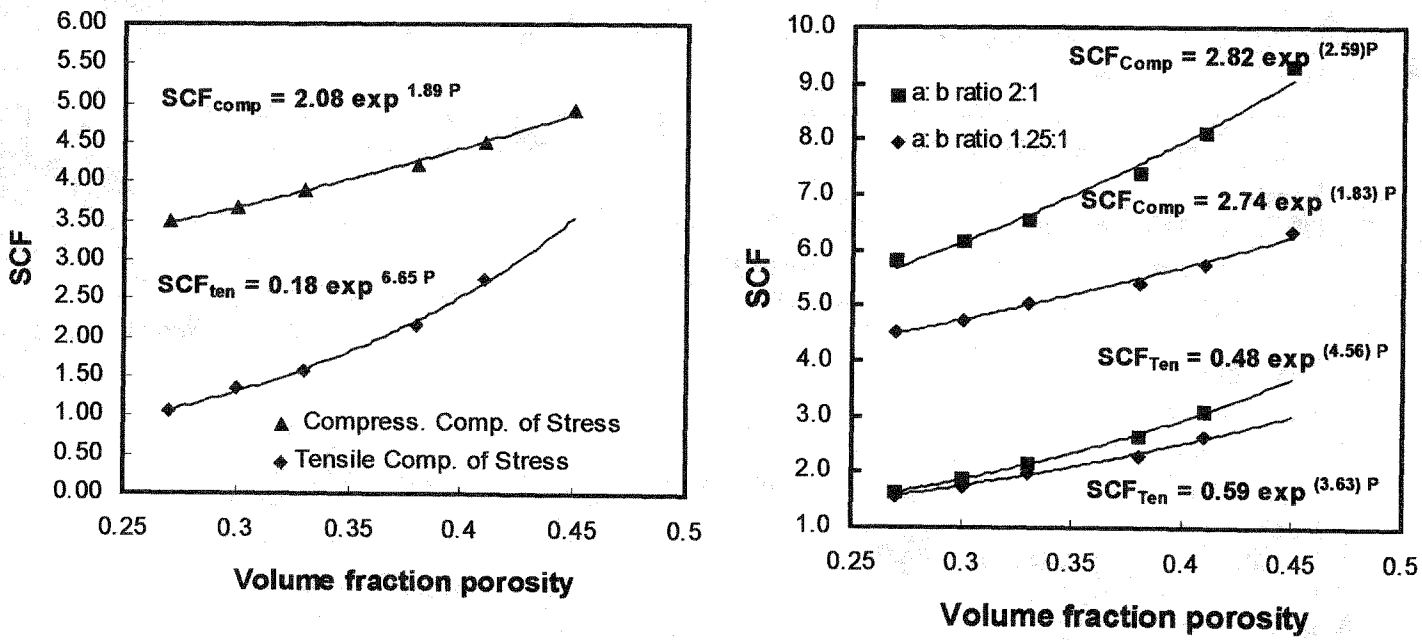

Fig. 9: **(a)** Effect of increasing porosity on the SCF for constant number of pores. **(b)** Variation of SCF with increasing porosity for constant pore shapes

Conclusions

Non-random porous ceramic structure can be processed indirectly from SFF process. Experimental results and statistical analysis show that the main parameters that affect the compressive strength of non-random porous ceramics are pore shape and distance between the pores in the horizontal plane. Since SFF process can control these parameters by changing the raster gap and road width, stronger porous structures can be produced via design optimization. Stress concentration effects by finite element modeling show similar behaviour as the failure strength trends obtained experimentally.

Acknowledgments

The authors would like to acknowledge the financial support from the Office of Naval Research under grant number N-00014-98-1-0550. The authors would also like to acknowledge the experimental help of Raj Atisivan, Susmita Bose and Sudarshan Rangaraj.

References

1. D. Hardy and D. J. Green, *J. Eur. Ceram. Soc.*, **15** (1995) 769.
2. R. M. de Souza, H. N. Yoshimura, C. Xavier and H. Goldenstein, *Key Engineering Materials* Vols. **127-131** (1997) 439.
3. E. W. White, J. N. Webber, D. M. Roy, E. L. Owen, R. T. Chiroff and R. A. White, *J. Biomed. Mater. Res. Symp.*, **6**, (1975) 23-7.
4. S. F. Hulbert, S. J. Morrison and J. J. Klawitter, *J. Biomed. Mater. Res. Symp.*, **6**, (1975) 347-74.
5. C. P. A. T. Klein, and P. Patka, Handbook of Bioactive Ceramics II: Calcium Phosphate and Hydroxylapatite Ceramics, edited by T. Yamamura, L. L. Hench and J. Wilson, CRC Press, Boca Raton, FL, (1990) 53-60.
6. T. Shrout, T., W. A. Schulze, and J. V. Biggers, *Mat. Res. Bull.* **14**, (1979) 1553-1559.
7. K. Rittenmyer, T. R. Shrout, W. A. Schulze, and R. E. Newnham, *Ferroelectrics* **41**, (1982) 189-195.
8. ---, "Rapid Prototyping Using FDM: A Fast, Precise, Safe Technology"; in Solid Freeform Fabrication Symposium Proceedings, Edited by H. L. Marcus, J. J. Beamen, J. W. Barlow, D L. Bourell, and R. H. Crawford. University of Texas at Austin, (1992) pp. 301-308.
9. A. Bandyopadhyay, R. K. Panda, V. F. Janas, M. K. Agarwala, S. C. Danforth and A. Safari, "Processing of Piezoelectric Ceramics by Fused Deposition Technique," *J. Am. Ceram. Soc.*, **80** 1366--72 (1997).
10. M. K. Agarwala, A. Bandyopadhyay, R. van Weeren, P. Whalen, Ahmad Safari and Stephen C. Danforth, "Fused Deposition of Ceramics: Rapid Fabrication of Structural Ceramic Components," *Ceram. Bull.*, **11** 60--65 (1996).
11. S. Bose, S Suguira and A Bandyopadhyay, " Processing of Controlled Porosity Ceramic Structures via Fused Deposition," *Scripta Materialia*, Accepted for Publication.
12. R. Ryshkewitch, "Compression Strength of Porous Sintered Alumina and Zirconia," *J. Am. Ceram. Soc.*, **36** [2] 65--68 (1953).
13. A. R. Boccaccini, G. Ondracek and E. Mombello, "Determination of Stress Concentration Factors in Porous Materials," *J. Mater. Sci. Letters*, **14** 534--536 (1995).
14. R.W. Rice, "Comparison of Physical Property-Porosity Behavior with Minimum Solid Area Models," *J. Mater. Sci.*, **31** 1509--1528 (1996).